

Regularized Wasserstein Means Based on Variational Transportation

Liang Mi, Wen Zhang, and Yalin Wang
 Arizona State University
 {liangmi, wzhan139, ylwang}@asu.edu

Abstract

We raise the problem of regularizing Wasserstein means and propose several terms tailored to tackle different problems. Our formulation is based on the variational transportation to distribute a sparse discrete measure into the target domain without mass splitting. The resulting sparse representation well captures the desired property of the domain while maintaining a small reconstruction error. We demonstrate the scalability and robustness of our method with examples of domain adaptation and skeleton layout.

1. Introduction

Aligning probability distributions is fundamental to many problems in computer vision and machine learning. From the early work on histogram manipulation, e.g. [40], to the recent work on generative modeling, e.g. [7], researchers have proposed various alignment techniques which benefit numerous fields including domain adaptation, e.g. [42], and shape registration, e.g. [32]. A universal approach to aligning probability distributions is through optimizing an objective function that measures the loss of the map between them. Regarding one distribution as the fixed target and the other the source, the alignment process in general follows an iterative manner where we alternatively update their correspondence and transform the source. When the source has much fewer samples or in a lower dimension, the process is essentially finding a sparse representation [8].

The optimal transportation (OT) loss, or the Wasserstein distance, has proved itself to be superiors in many aspects over several other measures [17, 6], benefiting various learning algorithms. By regarding the Wasserstein distance as a metric, researchers have been able to compute a sparse mean [21] of a distribution, which is a special case of the *Wasserstein barycenter* problem [1] when there is only one distribution. While optimal transportation algorithms find the correspondence between the distributions, updating the mean can follow the rule that each sample is mapped to the weighted average of its correspondence(s) [47].

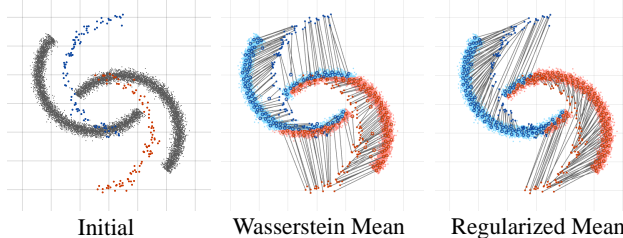


Figure 1. Regularized Wasserstein Means: An example from the two moons adaptation problem (rotation = 45°) showing the regularization by affine transformation. Regularized mean outperforms traditional mean by a large margin — 90.01% v.s. 75.90%

In this paper, we raise the problem of regularizing the *Wasserstein means*. In addition to finding a mean that yields the minimum transportation cost, in many cases we also want to insert certain properties so that it also satisfies other criteria. A common technique is adding regularization terms to the objective function. While most of the existing work, e.g. [12, 11], focus on regularizing the optimal transportation itself, we address the mean update rule and show the benefit from regularizing it. We introduce a new framework to compute OT-based sparse representation with regularization. We base our method on variational transportation [35] which produces a map between the source and the target distributions in a many-to-one fashion. Different from directly mapping the source into the weighted average of its correspondence [47, 11, 35], we propose to regularize the mapping with several regularization terms to cope with specific problems — domain adaptation and skeleton layout. The resulting mean, or centroid, can well represent the key property of the distribution while maintaining a small reconstruction error.

The rest of the paper is organized as follows: In Sec. 2 and 3, we relate our work with previous ones on OT and the Wasserstein barycenter/mean and provide core concepts in these areas; In Sec. 4, we show how to compute the Wasserstein means through variational OT; Sec. 5 presents our customized regularization terms for different problems; Sec. 6 reveals experiments showcasing the performance of regularized Wasserstein means; Finally, we conclude our work in Sec. 7 with discussion and future directions.

2. Related Work

2.1. Optimal Transportation

The optimal transportation (OT) problem was raised by Monge [36] in the 18th century, which sought a non-mass splitting transportation map between distributional data with the minimum cost. It resurfaced in 1940s when Kantorovich [26] introduced a relaxed version where mass *can* be split and provided the classic linear programming solution. A breakthrough for the non-mass splitting OT happened around 1990 when Brenier [9] proved its existence under quadratic cost. In more recent years, fast algorithms for computing, or approximating, OT have been proposed in both lines of research — mass splitting, e.g. [38, 12, 39] and non-mass splitting, e.g. [34, 20, 30, 27].

We follow Monge’s non-mass splitting formulation. Specifically, we adopt [35] to compute the OT because it gives clear paths of the samples, not a map that spreads out. Thus, we can insert the regularity into the path in a more elegant way — regularize the support instead of the mapping.

2.2. Wasserstein Barycenters and Means

The Wasserstein distance is the minimum cost induced by OT. In most cases, the cost itself may not be as desired as the map, but it satisfies all metric axioms [46] and thus often serves as the loss for matching distributions, e.g. [31, 28, 6]. Moreover, given multiple distributions, one can find their weighted average with respect to the Wasserstein metric. This problem was studied in [33, 3] for averaging two distributions and generalized to multiple distributions in [1], which defines it as the *Wasserstein barycenter* problem.

A special case of the barycenter problem is when there is only one distribution and we want to find its sparse discrete barycenter. Because computationally it is equivalent to the *k-means* problem, Ho *et al.* [21] defined it as the *Wasserstein means* problem. Even before that, Cuturi and Doucet had discussed it in [13] along with the connection of their algorithm to Lloyd’s algorithm in that case.

Our work focuses on regularizing the Wasserstein means. We obtain the mean by mapping the sparse points into the target domain according to the correspondence from the OT map. We insert regularization into the mapping process so that the sparse points not only have a small OT loss but they also have certain properties induced by the regularization terms. Our work should not be confused with other work on regularizing OT. For example, in [12] Cuturi introduced entropy-regularized OT where the entropy term controls the sparsity of the map and it was later used in [13] to compute Wasserstein barycenters. Courty *et al.* [11] also leveraged class labels to regularize OT for domain adaptation. These works only regularize OT and then directly update the support simply to the average of its correspondence. In this paper, we regularize the update.

3. Preliminaries

We begin with some basics on optimal transportation (OT). Suppose M is a compact metric space, $\mathcal{P}(M)$ is the space of all Borel probability measures on M and $\mu, \nu \in \mathcal{P}(M)$ are two such measures. A measure in the product space, $\pi(\cdot, \cdot) \in \mathcal{P}(M \times M)$, serves as a mapping between any two measures on M , i.e. $\pi: M \rightarrow M$. We define the cost function of the mapping as the geodesic distance $c(\cdot, \cdot): M \times M \rightarrow \mathbb{R}^+$.

3.1. Optimal Transportation

For a mapping $\pi(\mu, \nu)$ to be legitimate, the push-forward measure of one measure has to be the other one, i.e. $\pi_\# \mu = \nu$. Thus, for any measurable subsets $B, B' \subset M$ we have $\pi(B \times M) = \mu(B)$ and $\pi(M \times B') = \nu(B')$. We denote the space of all legitimate product measures by $\Pi(\mu, \nu) = \{\pi \in \mathcal{P}(M \times M) \mid \pi(\cdot, M) = \mu, \pi(M, \cdot) = \nu\}$.

Optimal transportation seeks a solution $\pi \in \Pi(\mu, \nu)$ that produces the minimum total cost:

$$W_p(\mu, \nu) \stackrel{\text{def}}{=} \left(\inf_{\pi \in \Pi(\mu, \nu)} \int_{M \times M} (c(x, y))^p d\pi(x, y) \right)^{\frac{1}{p}}, \quad (1)$$

where p indicates the finite moment of the cost function. The minimum cost is the *p-Wasserstein distance*. In this paper, we consider the 2-Wasserstein distance, W_2 .

Monge’s formulation restricts OT to preserve measures, that is, mass cannot be split during the mapping. Letting T denote such a mapping, $T: x \rightarrow y$, we have $d\pi(x, y) \equiv d\mu(x)\delta(y - T(x))$. Therefore, we formally define T as

$$T_{opt} = \arg \min_T \int_M c(x, T(x))^p d\mu(x). \quad (2)$$

In this paper, we follow (2). The details of the optimal transportation problem and the properties of the Wasserstein distance can be found in [45, 17]. With the abuse of notation, we use $\pi(\mu, \nu)$ to denote the OT map between measures μ and ν , and since the map is applied to their supports x and y we also use $\pi: x \rightarrow y$ and $y = \pi(x)$ to denote the map.

3.2. Variational Optimal Transportation

Suppose μ is continuous and ν is a set of Dirac measures in $M = \mathbb{R}^n$, supported on $\Omega_\mu = \{x \in M \mid \mu(x) > 0\}$ and $\Omega_\nu = \{y_j \in M \mid \nu_j > 0\}$, $j = 1, \dots, k$, and their total measures equal: $\text{vol}(\Omega) = \int_\Omega d\mu(x) = \sum_{j=1}^k \nu_j$. Gu *et al.* [20] proposed a variational solution to this *semi-discrete OT* on \mathbb{R}^n . It starts from a vector $\mathbf{h} = (h_1, \dots, h_k)^T$ and a piecewise linear function: $\theta_{\mathbf{h}}(x) = \max\{\langle x, y_j \rangle + h_j\}$, $j = 1, \dots, k$. Alexandrov proved in [2] that there exists a unique \mathbf{h} that satisfies the following constraint

$$\text{vol}(x \in \Omega \mid \nabla \theta_{\mathbf{h}}(x) = y_j) = \nu_j. \quad (3)$$

Furthermore, Brenier proved in [9] that $\nabla\theta_h: x \rightarrow y$ is the Monge's OT-Map if the transportation cost is the quadratic Euclidean distance $\|x - \nabla\theta_h(x)\|_2^2$.

Suppose $S_j(h) = \{x \in M \mid \nabla\theta_h(x) = y_j\}$ is the projection of θ_h on Ω . Variational OT (VOT) solves

$$\begin{aligned} E(\mathbf{h}) &\stackrel{\text{def}}{=} \int_{\Omega} \nabla\theta_h d\mu - \sum_{j=1}^k \nu_j h_j \\ &\equiv \int_{\mathbf{0}}^h \left(\sum_{j=1}^k \int_{\Omega \cap S_j(h)} d\mu \right) dh - \sum_{j=1}^k \nu_j h_j, \end{aligned} \quad (4)$$

and thus converts the OT problem into searching in a vector space $\mathcal{H} = \{h \in \mathbb{R}^k \mid \int_{\Omega \cap S_j(h)} d\mu > 0 \text{ for all } j\}$. Proved in [20], E (4) is convex in \mathcal{H} when $\sum_{j=1}^k h_j = 0$. The gradient of (4) is (3). Thus, minimizing (4) when its gradient approaches $\mathbf{0}$ will give us the desired \mathbf{h} , and the map $\nabla\theta_h$.

3.3. Wasserstein Barycenters

Given a collection of measures and weights $\{\mu_i, \lambda_i\}_{i=1}^N$, there exists such a measure ν that the weighted average of the Wasserstein distances between ν and all μ_i 's reaches the minimum. As exposed in [1], Aguech and Carlier defined such a problem as finding a barycenter in the measure space with respect to the Wasserstein distance:

$$\nu = \arg \min_{\nu \in \mathcal{P}_2(M)} \sum_{i=1}^N \lambda_i W_2^2(\nu, \mu_i).$$

Wasserstein barycenters of discrete measures in general exist for mass splitting OT but do not for non-mass splitting or measure-preserving OT. Yet, proved by Anderes *et al.* in [4], when the weights are uniform and all measures have finite number of supports, there still exists a barycenter ν that preserves the measure and whose number of supports $|\Omega_\nu|$ has a tight upper bound $|\Omega_\nu| \leq \sum_{i=1}^N |\Omega_{\mu_i}| - N + 1$, and the OT from every μ_i to ν preserves the measure.

Algorithm 1: Wasserstein Means

Input : $\mu(x) \in \mathcal{P}(M)$ and Dirac measures $\{\nu_j, y_j\}$
 $t = 0$.

repeat

- $\nu^{(t+1)} \leftarrow$ Update weight according to (7).
- $\pi^{(t+1)} \leftarrow$ Compute OT with fixed $y^{(t)}, \nu^{(t)}$.
- $y^{(t+1)} \leftarrow$ Update support according to (6).
- $t \leftarrow t + 1$.

until convergence.

return π, y, ν .

4. Wasserstein Means via Variational OT

A special case of the Wasserstein barycenters problem is when $N = 1$. In that case, we are computing a barycenter of a single probability measure. We call it the *Wasserstein mean* (WM). Beyond a special case, the barycenters and the means have the following connection.

Proposition 1. *Given a compact metric space M , a transportation cost $c(\cdot, \cdot): M \times M \rightarrow \mathbb{R}^+$, and a collection of Borel probability measures $\mu_i \in \mathcal{P}(M)$, with weights λ_i , $i = 1, \dots, N$, the Wasserstein mean ν_m of their average measure induces a lower bound of the average Wasserstein distance from the barycenter ν_b to them, provided that $|\Omega_{\nu_b}| \leq |\Omega_{\nu_m}| \leq k$ for some finite k .*

Proof. Since $W_2^2(\nu_b, \cdot)$ is convex for its metric property, according to Jensen's inequality, we have

$$W_2^2(\nu_b, \sum_{i=1}^N \lambda_i \mu_i) \leq \sum_{i=1}^N \lambda_i W_2^2(\nu_b, \mu_i).$$

Then, according to Wasserstein mean's definition,

$$W_2^2(\nu_m, \sum_{i=1}^N \lambda_i \mu_i) \leq W_2^2(\nu_b, \sum_{i=1}^N \lambda_i \mu_i), \quad \forall \nu_b.$$

The result shows. The equal sign holds when $N = 1$. \square

We should point out that if $\{\mu_i\}$ are discrete measures, then for the barycenter to exist we need to add the condition from [4] that $|\Omega_{\nu_b}| \leq \sum_{i=1}^N |\Omega_{\mu_i}| - N + 1$, which also bounds $|\Omega_{\nu_m}|$ through $|\Omega_{\nu_m}| \leq \sum_{i=1}^N |\Omega_{\mu_i}|$.

Now, approaching Wasserstein means is essentially through optimizing the following objective function:

$$\begin{aligned} \min f(\pi, y, \nu) &\stackrel{\text{def}}{=} \min_{\pi, y_j, \nu_j} \sum_{j=1}^k \sum_{y_j=\pi(x)} \mu(x) \|y_j - x\|_2^2, \\ \text{s.t. } \nu_j &= \sum_{y_j=\pi(x)} \mu(x). \end{aligned} \quad (5)$$

When y and ν are fixed, (5) becomes a classic optimal transportation problem and we adopt variational optimal transportation (VOT) [35] to solve it.

Then, it boils down to solving for y and ν . Certainly (5) is differentiable at all $y \in \mathbb{R}^{n \times k}$ and is convex. It's optimum w.r.t. y can be achieved at

$$\tilde{y}_j = \frac{\int_{\Omega_\mu \cap S_j} x d\mu(x)}{\int_{\Omega_\mu \cap S_j} d\mu(x)}. \quad (6)$$

It is essentially to update the mean to the centroid of corresponding measures, adopted in for example [13, 47, 11]. The slight difference in our method is that VOT is non-mass

splitting and thus the centroid in our case has a clear position without the need for weighting.

As discussed in [13], (5) is not differentiable w.r.t. ν . However, we can still get its optimum through the following observation.

Observation 1. *The critical point of the function $\nu \rightarrow f(\pi, \nu)$ is where ν induces π being the gradient map of the unweighted Voronoi diagram formed by ν 's support y . In that case, every empirical sample $\mu(x)$ at x is mapped to its nearest y_j , which coincides with Lloyd's algorithm.*

Proof. Suppose ν induces the OT map π that is from x to its nearest y_j for all x . Then, the transport map $\pi': x \rightarrow y_{j'}$ that satisfies any other $\nu' = \int_{\Omega \cap S_j} d\mu(x)$ will yield an equal or larger cost $\int_{\Omega} \|y_j - x_i\|_2^2 d\mu(x_i) \leq \int_{\Omega} \|y_{j'} - x_i\|_2^2 d\mu(x_i)$. \square

Thus, we can write the update rule for ν as

$$\tilde{\nu}(y_j) = \int_{\Omega \cap S_j} d\mu(x), \quad (7)$$

$$\text{s.t. } S_j = \{x \in M \mid \|x - y_j\|_2 \leq \|x - y_i\|_2, i \neq j\}.$$

Updating the three parameters π , y , and ν can follow the *block coordinate descent* method. Since at each iteration we have closed-form solutions in the y and ν directions, there is no need to do a line search there. We wrap up our algorithm for computing the Wasserstein means in Alg. 1

As discussed in [13], when $N = 1$ and $p = 2$, computing the Wasserstein barycenter (in this case the Wasserstein mean) is equivalent to Lloyd's algorithm for solving the k-means problem. The difference also occurs when we have a constraint on the weight $\nu_j(y)$. Ng [37] considered a uniform weight for all S_j . Our algorithm can adapt to any constraint on $\nu_j \geq 0$. In this case, our algorithm is equivalent to [13] where the update of the support is equivalent to re-centering it by our (6).

Algorithm 2: Regularized Wasserstein Means

```

Input :  $\mu(x) \in \mathcal{P}(M)$ ,  $\{\nu_j, y_j\}$ 
 $t = 0$ .
repeat
   $\pi^{(t+1)} \leftarrow$  Compute OT  $\pi(\mu, \nu)$  with fixed  $y^{(t)}$ .
   $\tilde{y} \leftarrow$  Compute new centroid according to (6).
  repeat
     $| \quad y^{(t+1)} \leftarrow$  Update centroid by optimizing (10).
  until  $y^{(t+1)}$  converges.
   $t \leftarrow t + 1$ .
until  $\pi$  and  $y$  converge.
return  $\pi, y$ .

```

5. Regularized Wasserstein Means

In many problems of computer vision and machine learning, the solution that comes purely from the perspective of the mapping cost may not serve the best to represent the data or it could cause overfitting. Regularization is a common technique to introduce desired properties in the solution. In the previous section, we talked about the Wasserstein means problem and its optimizers: OT $\pi(\nu, \mu)$, support y , and the measure $\nu(y)$. In this section, we detail our strategies to regularize y along with several regularization terms that we propose to penalize the Wasserstein means cost. For simplicity, we fix the given $\nu(y)$ and only consider π and y in the *regularized Wasserstein means* (RWM) problem.

We start with a general loss function:

$$\begin{aligned} \mathcal{L}(\pi, y) &= \mathcal{L}_{\text{ot}}(\pi, y) + \lambda \mathcal{L}_{\text{reg}}(y), \\ \mathcal{L}_{\text{ot}}(\pi, y) &= \int_{\Omega} \|y - x\|_2^2 d\mu(x), \text{ s.t. } y = \pi(x). \end{aligned} \quad (8)$$

We call the first term the *OT loss*. Our goal here is to explore $\mathcal{L}_{\text{reg}}(y)$ and the use of it. Optimizing (8) can also follow the block coordinate descent method. First, we fix the mean and compute the OT. Unlike in Alg. 1 where we directly update the mean to the average of their correspondences, next, we regularize the mean to satisfy certain properties through local minimization on (8).

Minimizing the OT loss $\mathcal{L}_{\text{ot}}(\pi, y)$ w.r.t. y can be simplified to minimizing the quadratic loss for each support to its estimate, i.e. $\mathcal{L}_{\tilde{y}} = \sum_j \|y_j - \tilde{y}_j\|_2^2$, since they are equivalent to each other:

$$\begin{aligned} \int_{S_j} \|y_j - x\|_2^2 d\mu(x) &= (y_j^2 - 2y_j \int_{S_j} x d\mu(x) + C_1) \\ &= \|y_j - \int_{S_j} x d\mu(x)\|_2^2 + C_2 = \|y_j - \tilde{y}_j\|_2^2 + C_2. \end{aligned} \quad (9)$$

C_1, C_2 are some constants. \tilde{y}_j is from (6) and S_j is the set in which x is mapped to y_j . It is defined by VOT as $S_j = \{x \in M \mid \langle y_j, x \rangle - h_j \geq \langle y_i, x \rangle - h_i, \forall i \neq j\}$, see Sec. 3.2. Thus, we re-write (8) as

$$\mathcal{L}(\pi, y) = \sum_j \|y_j - \tilde{y}_j\|_2^2 + \lambda \mathcal{L}_{\text{reg}}(y) \quad (10)$$

We provide the general algorithm to compute regularized Wasserstein means in Alg. 2. For optimizing (10), we borrow the solvers from Spiii [41] and SciPy [24] for C++ and Python implementations, respectively. Code is available at <https://github.com/icemiliang/pivot>

Citing the convergence proof from Grippo and Sciandrone [19], as long as we add a convex regularization term, because $\pi: x \rightarrow y$ is compact and convex, our 2-block coordinate descent-based algorithm indeed will converge. In the rest of this section, we discuss in detail several regularization terms based on potential energy, kernels in general, affine transformation, and length and curvature.

5.1. Potential Energy Empowered by Class Labels

We begin with a fair assumption that samples within the same class reside closer to each other and samples that belong to different classes are relatively far away from each other. This behavior can be expressed by the potential energy between any two samples. Given that, we propose to regularize the mean update process by adding a signed distance between every two samples, promoting intra-class connection and discouraging inter-class connections. To this end, we define the regularization term as

$$\lambda \mathcal{L}_{\text{reg}}(y) = \lambda_1 \sum_{\substack{i \neq j \\ l_i = l_j}} \|y_i - y_j\|_2^2 - \lambda_2 \sum_{\substack{i \neq j \\ l_i \neq l_j}} \|y_i - y_j\|_2^2, \quad (11)$$

where l_i and l_j are the labels of y_i and y_j . In this way, those samples that share the same label attract each other and those that belong to different classes repel each other.

If we remove the second term of (11), then, it becomes convex, leading to a convex (10). Thus, we choose only adopt the first term and propose the following loss function for regularizing class labels:

$$\mathcal{L}(\pi, y) = \sum_j \|y_j - \tilde{y}_j\|_2^2 + \lambda \sum_{i \neq j} \|y_i - y_j\|_2^2 \delta(l_i - l_j). \quad (12)$$

$\delta(\cdot)$ is the Delta function. Intuitively, we are only promoting the intra-class connection and yet this brings much convenience for optimization. Similar regularization terms have also been used in [11].

5.2. Kernels and Beyond

From a computational point of view, (11) expresses a regularization by the loss of a linear kernel that measures pair-wise similarities. Thus, a natural thought is to extend it to a general kernel-regularized loss. We write it as

$$\mathcal{L}_{\text{reg}}(y) \stackrel{\text{def}}{=} g(y) = \sum_{i,j=1}^k (\alpha_{ij} K(y_i, y_j)) + \beta. \quad (13)$$

By carefully designing α and β , we can leverage the pair-wise similarity loss to regularize the motion of y . Recall that the goal of the regularizer is to differentiate y according to their labels. Therefore, when y are fixed, solving for the optimal α and β is equivalent to solving for an optimal support vector machine (SVM) with the kernel $K(y_i, y_j)$.

In light of the above discovery, we raise the problem of

$$\min_{\pi, y} W(\nu, \mu) + \lambda g(y), \quad (14)$$

combining OT and SVM. By solving OT, we align different domains; by solving SVM, we leverage the class information to regularize the alignment. To maintain an unsupervised fashion, we only leverage the class information of the

source domain. Given fixed mean and its labels $\{y_i, l_i\}$, we can follow the SMO algorithm and solve for an optimal SVM and obtain a subset of the centroids, $y_{SV} \subseteq y$ with associated $\{\alpha_i\}$ as the supporting vectors. These vectors will serve in (13) and (14) to regularize the displacement of y in the next iteration.

Let us briefly compare our approach with a similar work. Courty *et al.* proposed JDOT [10] which computes a joint probability of samples and labels. They incorporate a general learning function “ f ” into the formulation. They leverage mass-splitting OT and regard the correspondences as the weighting function of the label loss. Because we use non-mass splitting OT, the label of the target domain is automatically determined by the many-to-one correspondence. Thus, learning functions cannot be applied to the target domain but only to the mean supports. This difference also fits the different goals of the two methods. The goal of JDOT is to learn a classifier and thus the source domain is not moving during the OT or learning process. Our goals, however, is to learn a proper transformation of the mean into the target domain and thus a good classifier on the target domain becomes less important.

5.3. Affine Transformations

While OT recovers a transformation between two domains that induces the lowest cost, it does not consider the structure within the domains. Pre-assuming a type of the transformation and then estimating its parameters is one of the popular approaches to solving domain alignment-related problems, for example in [15, 18, 11]. In this way, the structure of the domain can be preserved to some extent. Let us follow this trend and assume that two domains can be matched by an affine transformation with modifications, that is, any transformation between domains is a combination of an affine and a small non-affine transformations. This leads to our following strategy that we on the one hand regularize the mean to be roughly an affine transformation in order to preserve the structure of the domain during the mapping but on the other hand also allow OT to adjust the mapping so that it can recover non-affine transformations.

We follow Alg. 2. First, we compute OT to obtain the target mean positions $\tilde{y} = \pi(x)$ and use the paired means $\{y, \tilde{y}\}$ to determine the parameters of an affine transformation A subject to $\tilde{y} = Ay$ through a least squares estimate. Suppose $y_j^A = Ay$ is the estimate purely based on the affine transformation, then, we have the RWM loss

$$\mathcal{L}(\pi, y) = \sum_j \|y_j - \tilde{y}_j\|_2^2 + \lambda \sum_j \|y_j - y_j^A\|_2^2. \quad (15)$$

Similarly, we can assume other types of transformations, either weaker or stronger than affine, such as perspective and rigid transformations.

5.4. Length and Curvature

The nature of many-to-one mapping in the WM problem enables itself to be suitable for skeleton layout. Consider a 3D thin, elongated point cloud. Our goal is to find a 3D curve consisting of sparse points to represent the shape of the cloud. The problem with directly using WM for skeleton layout is that the support is unstructured. Therefore, we propose to pre-define the topology of the curve and add the length and curvature to regularize its geometry, both intrinsically and extrinsically.

We give an order of the support so that they can form a piece-wise linear curve $\gamma(y)$ approximating the real one. Its length is approximated by summarizing the length segment

$$\int_0^{length} ds = \int_0^1 \|\gamma'(y)\| dy \approx \sum_{1 \leq i < k} \|y_i - y_{i+1}\|,$$

and its curvature $k(y_i) = \frac{\|\gamma'(y_i) \times \gamma''(y_i)\|}{\|\gamma'(y_i)\|^3}$ at point y_i can be approximated in the same way as in [44], which is to compute the total curvature of the B-spline segment fitted to three adjacent supports. Thus, the regularization on the length and curvature can express itself as follows:

$$\begin{aligned} \lambda \mathcal{L}_{\text{reg}} &= \lambda \left(\sum_{1 \leq i < k} \|y_i - y_{i+1}\|_2 + \sum_{1 < i < k} k(y_i) \right) \\ &\equiv \lambda_1 \sum_{1 \leq i < k} g(\gamma'(y_i)) + \lambda_2 \sum_{1 < i < k} l(\gamma''(y_i)). \end{aligned} \quad (16)$$

where $g(\cdot)$ and $l(\cdot)$ are some function computed out of the length and curvature. We could go further and include torsion into the term but since we do not pursue a perfectly smooth curve but rather the reasonable embedding of the supports in the interior of the point cloud, we have passed torsion. Finally, we propose the the following regularized clustering loss for skeleton layout:

$$\begin{aligned} \mathcal{L}(\pi, y) &= \sum_j \|y_j - \tilde{y}_j\|_2^2 \\ &+ \lambda_1 \sum_{1 \leq i < k} g(\gamma'(y_i)) + \lambda_2 \sum_{1 < i < k} l(\gamma''(y_i)). \end{aligned} \quad (17)$$

(17) belongs to a general framework for skeleton extraction discussed in [22].

In case we have shapes with branching, we can easily extend (17) considering the skeleton as a whole when computing the OT and regularizing each branch separately. We can also include circles each as a separate branch. Suppose, now, the skeleton $\Gamma = \{\gamma_j\}$ is a set of 1-D curves. Then, the overall loss in this case will be

$$\begin{aligned} \mathcal{L}(\pi, y) &= \sum_j \|y_j - \tilde{y}_j\|_2^2 \\ &+ \sum_{\gamma \in \Gamma} \left(\lambda_1 \sum_{1 \leq i < k} g(\gamma'(y_i)) + \lambda_2 \sum_{1 < i < k} l(\gamma''(y_i)) \right). \end{aligned} \quad (18)$$

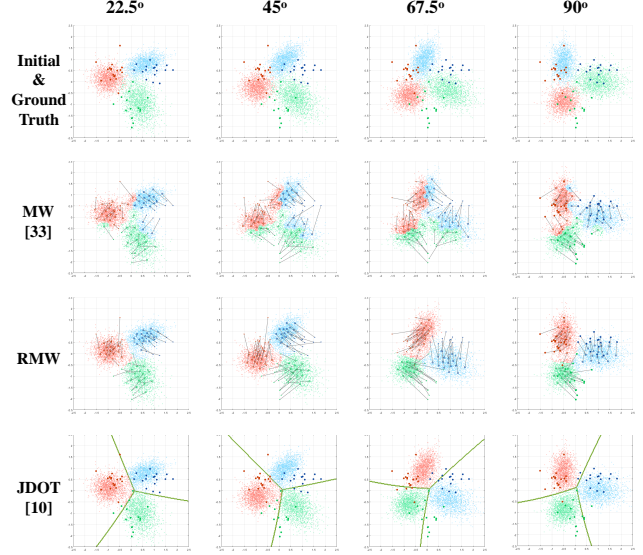


Figure 2. Regularizing the WM by the intra-class potential energy can adapt it to domains that suffer unknown rotations.

6. Applications

In this section, we demonstrate the use of RWM in domain adaptation and skeleton layout.

6.1. Domain Adaptation

Domain adaptation comprises three experiments. The 1st one shows the use of the linear kernel weighted by class labels. The 2nd one shows results from two moons testing affine transformation. In the 3rd one, we apply RWM to the adaptations between the MNIST and the USPS datasets.

6.1.1 Simulation with Gaussian mixtures

Suppose a Gaussian mixture has three components with different parameters, each belongs to a different class as shown in three colors in Fig. 2. We rotate the mixture by a certain degree to emulate an unknown shift of the domain and apply our method to recover the shift. We hold the assumption that samples from the same class reside closer to each other and apply RWM regularized by class labels.

We sample the source domain 50 times and the target domain 5,000 times at 22.5°, 45°, 67.5°, and 90°. Fig. 2 top row shows the setups. Colors indicate the ground truth. The 2nd row shows the result from computing the WM without regularization as in [35]. The 3rd row shows our result. Before 60°, our method can well drive source samples into the correct target domain. The lighter colors on the target samples in the 2nd and 3rd rows indicate the predicted class by using the OT correspondence. Since our OT preserves the measure during the mapping, we can deterministically label each unknown sample by querying its own centroid's

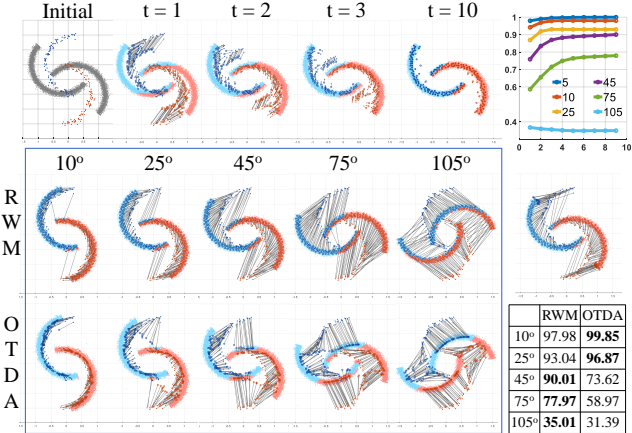


Figure 3. RWM: 1st row performance over iteration under 20°; 2nd and 3rd rows performance under different degrees; 2nd row right RWM gets better accuracy if weights of tails reduced.

class. Note, that this is different from the 1NN classification algorithm. 1NN assigns the label according to the nearest neighbor at the Euclidean distance, while our assignment rule is based on the power distance [35]. Only when the weight of every centroid equals each other will the power distance coincide with the Euclidean distance. In the last row, we show the result from [10]. It learns an RBF SVM classifier on the target samples. Both [10] and ours cannot adapt to more than 60°, which is reasonable.

6.1.2 Simulation with Two Moons

We use the two moons dataset to break down the learning process of RWM and also to demonstrate the regularization by an affine transformation. Fig. 3 shows the learning process. The known domain contains 200 samples plotted in blue and red dots. The unknown domain is the known after a rotation. We sample the unknown domains 10,000 times. The top row shows the result on the 20° case after each iteration. At each step, all the samples roughly share an affine transformation and they also have local differences. In the end, RWM almost recovers the rotation transformation with a small error. Top right shows accuracy over iterations under different degrees. The 2nd row shows the result under different degrees of rotation. We weight in OTDA-GL's result [11, 16] in the 3rd row showing that our method outperforms OTDA under a large rotation. Besides, RWM maps the samples *into* the domain which OTDA fails to.

To show the impact of the weights of the samples, and also to humor the readers, we repeat the 45° and give the source samples different weights. In practice, the weight can be some uncertainty score that indicates samples' credibility or influence. Let us decrease the weights on the tails of the moons for some reason. The middle right plot shows a better result than the original one 94.72% v.s. 90.01%.



Figure 4. Sample images from the MNIST and the USPS datasets.

6.1.3 Digit Classification

We evaluate our method on handwriting digit datasets to test its applicability to real data of high dimensionality. We adopt the same strategy we discussed in Sec. 6.1.1. We map the source domain with labels into the target domain and directly index each target sample as we did in 6.1.1 and 6.1.2.

Datasets MNIST [29] containing in total 70,000 grayscale images of 10 classes each having about 7,000 samples. USPS [23] containing 9,293 grayscale images of 10 classes each having from 708 to 1553 samples. Fig. 4 shows some sample images. We resample the MNIST images to the same size of 16 × 16 with the USPS images.

Features We use two separate features to represent the images — (i) normalized 256-dimensional image pixels and (ii) the feature extracted from the last fully connected layer of a modified LeNet 5 [29] as implemented in [43]. It has 500 dimensions. We regard LeNet as an encoder.

Tasks (i) *USPS → MNIST* Due to the imbalance across the datasets, we transfer the domain in a bootstrapping manner. We repeat the tests 3 times. Each time we randomly select 708 samples from each class of USPS and fully train LeNet with them and extract the features. Then, we obtain the LeNet features of all the MNIST by directly applying the fixed encoder to the MNIST images. Finally, we apply different methods to those features for adaptation.

(ii) *MNIST → USPS* Similarly, we randomly sample MNIST images according to the population of each class in USPS. For example, there are 1,553 “0”s and 852 “4”s in USPS and we thus choose 155 “0”s and 85 “4”s from MNIST. The rest of the task follows (i).

Methods 1NN, ADDA [43], OTDA [11], and RWM.

Results Tab. 1 shows the results. RWM outperforms OTDA but loses to ADDA, probably because that neural networks can emulate arbitrary transformations while our mapping is roughly a diffeomorphism because of VOT [20]. We hypothesis that in these spaces the MNIST and USPS domains cannot be aligned together by a diffeomorphism.

Table 1. Classification Accuracy (%) on MNIST \leftrightarrow USPS

Task	Feature	1NN	ADDA	OTDA	RWM
USPS	Image	29.79	n/a	59.74	68.79
→ MNIST	LeNet	29.97	88.23	67.85	66.57
MNIST	Image	57.84	n/a	72.42	77.13
→ USPS	LeNet	40.35	87.69	74.54	74.88

6.2. Skeleton Layout

We follow a similar setup as in [39]. Suppose we have a point cloud $\mu \in \mathcal{P}(M = \mathbb{R}^3)$ and a graph $G = (V, E)$ representing the topology of the shape that the cloud is reflecting. Then, the skeleton layout problem is finding particular embeddings of the nodes $y(\nu) : \nu \rightarrow \mathbb{R}^3$ that can relate the skeleton to the geometry of the point cloud. From a computational point of view, we can regard the skeleton as a regularized mean of the point cloud. On the one hand, we expect the skeleton to have (i) a small reconstruction error with the original cloud; on the other hand, the skeleton itself has to have (ii) a clear shape and (iii) certain smoothness. The three terms of (18) respectively satisfy these requirements.

Now, consider the human shape point cloud [5] in Fig. 5 top left. We initial a rough embedding of a graph by fixing its ends $V_0 \subset V$ to certain known positions $y_{\nu \in V_0}$ which are head, hands, and feet in this example, and set the rest of nodes evenly distribute along their branch. Our goal is to embed the nodes $\nu \in V \setminus V_0$ in this \mathbb{R}^3 space by applying (18). Because the weight of each centroid determines its boundaries with other centroids, it has to be adjusted to the local density of the point cloud so that all the centroids could lay on the skeleton with roughly an even interval in between. Thus, we relax the restriction on weight and reinstate (7). To prevent it from quickly trapped into a local minimum, we update the weight by momentum gradient descent, $\nu(y_j)^{(t+1)} \leftarrow \lambda \nu(y_j)^{(t)} + (1 - \lambda) \int_{\Omega \cap S_j} d\mu(x)$.

Top right of Fig. 5 shows the result from our algorithm. The generated skeleton successfully captures the shape of the human body. We color the skeleton nodes according to their position in the graph and the color the point cloud indicating their OT correspondences to the skeleton. We compare the result with no regularization in the third column. We also show Lloyd's k-means algorithm in the second column. We add regularization to Lloyd's algorithm to make it a fair comparison. Because in the cloud there are a few more samples in the right "waist" than in the left, Lloyd's algorithm pushes the skeleton to the right a little bit.

In addition, we test the robustness of our method under different initial conditions. The second row (b) shows results from a different initial by adding noise and the third row (c) shows the result with an extreme initial condition. We algorithm eventually recovers a coherent, correct shape, but without the regularization we could end up with "ill-posed" embeddings. The last row (d) presents on the left another example from the Armadillo model [25]. In the bottom right, we show the result from [39]. [39] regards the problem as a *Wasserstein propagation* problem and adopted Wasserstein barycenter techniques to relate the samples of the cloud to the graph, which is much heavier. The average time of 5 trials spent on computing the skeleton for [39] was 1,200 seconds while our algorithm took 15 seconds on average. CPU: Intel i5-7640x 4.0 GHz.

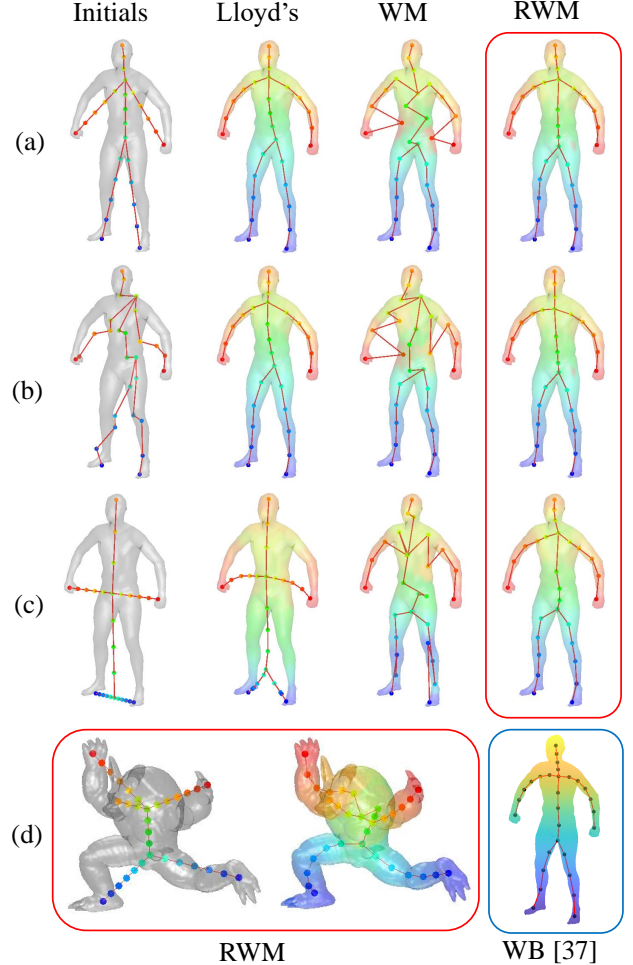


Figure 5. Skeleton layout. Embedding a sparse curve in the 3D cloud domain. By fixing the ending points, RWM embeds of a predefined graph that relates to the shape of the cloud. It is robust to noises and different initial positions and more efficient than computing Wasserstein barycenters (WB).

7. Discussion

We have talked about the Wasserstein means problem and our method to regularize it. The results have shown that our method can well adapt to different problems by adopting different regularization terms. This work opens up a new perspective to look at the Wasserstein means problem, or the k-means problem.

In this paper, we adopted VOT to obtain the OT map. In general, other OT solvers, e.g. Sinkhorn distances, could also work in our framework. In that case, we need to compute the weighted centroid to update the support. In [14], OT has been inserted into a neural network's loss function for aligning different domains, which could guide the following work to enrich deep neural networks by OT techniques including ours. Future work could also include regularizing Wasserstein barycenters.

References

[1] M. Aguech and G. Carlier. Barycenters in the Wasserstein space. *SIAM Journal on Mathematical Analysis*, 43(2):904–924, 2011. 1, 2, 3

[2] A. D. Alexandrov. *Convex polyhedra*. Springer Science & Business Media, 2005. 2

[3] L. Ambrosio, N. Gigli, and G. Savaré. *Gradient flows: in metric spaces and in the space of probability measures*. Springer Science & Business Media, 2008. 2

[4] E. Anderes, S. Borgwardt, and J. Miller. Discrete Wasserstein barycenters: Optimal transport for discrete data. *Mathematical Methods of Operations Research*, 84(2):389–409, 2016. 3

[5] D. Anguelov, P. Srinivasan, D. Koller, S. Thrun, J. Rodgers, and J. Davis. Scape: shape completion and animation of people. In *ACM transactions on graphics (TOG)*, volume 24, pages 408–416. ACM, 2005. 8

[6] M. Arjovsky, S. Chintala, and L. Bottou. Wasserstein GAN. *arXiv preprint arXiv:1701.07875*, 2017. 1, 2

[7] C. Beecks, A. M. Ivanescu, S. Kirchhoff, and T. Seidl. Modeling image similarity by Gaussian mixture models and the signature quadratic form distance. In *Computer Vision (ICCV), 2011 IEEE International Conference On*, pages 1754–1761. IEEE, 2011. 1

[8] Y. Bengio, A. Courville, and P. Vincent. Representation learning: A review and new perspectives. *IEEE transactions on pattern analysis and machine intelligence*, 35(8):1798–1828, 2013. 1

[9] Y. Brenier. Polar factorization and monotone rearrangement of vector-valued functions. *Communications on pure and applied mathematics*, 44(4):375–417, 1991. 2, 3

[10] N. Courty, R. Flamary, A. Habrard, and A. Rakotomamonjy. Joint distribution optimal transportation for domain adaptation. In *Advances in Neural Information Processing Systems*, pages 3730–3739, 2017. 5, 7

[11] N. Courty, R. Flamary, D. Tuia, and A. Rakotomamonjy. Optimal transport for domain adaptation. *IEEE transactions on pattern analysis and machine intelligence*, 39(9):1853–1865, 2017. 1, 2, 3, 5, 7

[12] M. Cuturi. Sinkhorn distances: Lightspeed computation of optimal transport. In *Advances in neural information processing systems*, pages 2292–2300, 2013. 1, 2

[13] M. Cuturi and A. Doucet. Fast computation of Wasserstein barycenters. In *International Conference on Machine Learning*, pages 685–693, 2014. 2, 3, 4

[14] B. B. Damodaran, B. Kellenberger, R. Flamary, D. Tuia, and N. Courty. Deepjdot: Deep joint distribution optimal transport for unsupervised domain adaptation. *arXiv preprint arXiv:1803.10081*, 2018. 8

[15] B. Fernando, A. Habrard, M. Sebban, and T. Tuytelaars. Unsupervised visual domain adaptation using subspace alignment. In *Proceedings of the IEEE international conference on computer vision*, pages 2960–2967, 2013. 5

[16] R. Flamary and N. Courty. POT Python optimal transport library, 2017. 7

[17] A. L. Gibbs and F. E. Su. On choosing and bounding probability metrics. *International statistical review*, 70(3):419–435, 2002. 1, 2

[18] R. Gopalan, R. Li, and R. Chellappa. Domain adaptation for object recognition: An unsupervised approach. In *Computer Vision (ICCV), 2011 IEEE International Conference on*, pages 999–1006. IEEE, 2011. 5

[19] L. Grippo and M. Sciandrone. On the convergence of the block nonlinear Gauss–Seidel method under convex constraints. *Operations research letters*, 26(3):127–136, 2000. 4

[20] X. Gu, F. Luo, J. Sun, and S.-T. Yau. Variational principles for Minkowski type problems, discrete optimal transport, and discrete Monge–Ampere equations. *arXiv preprint arXiv:1302.5472*, 2013. 2, 3, 7

[21] N. Ho, X. Nguyen, M. Yurochkin, H. H. Bui, V. Huynh, and D. Phung. Multilevel clustering via Wasserstein means. *arXiv preprint arXiv:1706.03883*, 2017. 1, 2

[22] H. Huang, S. Wu, D. Cohen-Or, M. Gong, H. Zhang, G. Li, and B. Chen. L1-medial skeleton of point cloud. *ACM Trans. Graph.*, 32(4):65–1, 2013. 6

[23] J. J. Hull. A database for handwritten text recognition research. *IEEE Transactions on pattern analysis and machine intelligence*, 16(5):550–554, 1994. 7

[24] E. Jones, T. Oliphant, P. Peterson, et al. SciPy: Open source scientific tools for Python, 2001–. [Online; accessed 1today]. 4

[25] E. Kalogerakis, A. Hertzmann, and K. Singh. Learning 3d mesh segmentation and labeling. *ACM Transactions on Graphics (TOG)*, 29(4):102, 2010. 8

[26] L. V. Kantorovich. On the translocation of masses. In *Dokl. Akad. Nauk SSSR*, volume 37, pages 199–201, 1942. 2

[27] S. Kolouri, Y. Zou, and G. K. Rohde. Sliced wasserstein kernels for probability distributions. In *Proceedings of the IEEE Conference on Computer Vision and Pattern Recognition*, pages 5258–5267, 2016. 2

[28] M. Kusner, Y. Sun, N. Kolkin, and K. Weinberger. From word embeddings to document distances. In *International Conference on Machine Learning*, pages 957–966, 2015. 2

[29] Y. LeCun, L. Bottou, Y. Bengio, and P. Haffner. Gradient-based learning applied to document recognition. *Proceedings of the IEEE*, 86(11):2278–2324, 1998. 7

[30] B. Lévy. A numerical algorithm for L2 semi-discrete optimal transport in 3d. *ESAIM: Mathematical Modelling and Numerical Analysis*, 49(6):1693–1715, 2015. 2

[31] H. Ling and K. Okada. An efficient earth mover’s distance algorithm for robust histogram comparison. *IEEE transactions on pattern analysis and machine intelligence*, 29(5):840–853, 2007. 2

[32] J. Ma, J. Zhao, and A. L. Yuille. Non-rigid point set registration by preserving global and local structures. *IEEE Transactions on image Processing*, 25(1):53–64, 2016. 1

[33] R. J. McCann. A convexity principle for interacting gases. *Advances in mathematics*, 128(1):153–179, 1997. 2

[34] Q. Mérigot. A multiscale approach to optimal transport. In *Computer Graphics Forum*, volume 30, pages 1583–1592. Wiley Online Library, 2011. 2

- [35] L. Mi, W. Zhang, X. Gu, and Y. Wang. Variational Wasserstein clustering. In *Proceedings of the European Conference on Computer Vision (ECCV)*, pages 322–337, 2018. [1](#), [2](#), [3](#), [6](#), [7](#)
- [36] G. Monge. Mémoire sur la théorie des déblais et des remblais. *Histoire de l'Académie Royale des Sciences de Paris*, 1781. [2](#)
- [37] M. K. Ng. A note on constrained k-means algorithms. *Pattern Recognition*, 33(3):515–519, 2000. [4](#)
- [38] J. Rabin, G. Peyré, J. Delon, and M. Bernot. Wasserstein barycenter and its application to texture mixing. In *International Conference on Scale Space and Variational Methods in Computer Vision*, pages 435–446. Springer, 2011. [2](#)
- [39] J. Solomon, F. De Goes, G. Peyré, M. Cuturi, A. Butscher, A. Nguyen, T. Du, and L. Guibas. Convolutional wasserstein distances: Efficient optimal transportation on geometric domains. *ACM Transactions on Graphics (TOG)*, 34(4):66, 2015. [2](#), [8](#)
- [40] J. A. Stark. Adaptive image contrast enhancement using generalizations of histogram equalization. *IEEE Transactions on image processing*, 9(5):889–896, 2000. [1](#)
- [41] P. Strandmark. A library for unconstrained minimization of smooth functions using Newton’s method or L-BFGS. <https://github.com/PetterS/spii>. [4](#)
- [42] B. Sun and K. Saenko. Deep coral: Correlation alignment for deep domain adaptation. In *European Conference on Computer Vision*, pages 443–450. Springer, 2016. [1](#)
- [43] E. Tzeng, J. Hoffman, K. Saenko, and T. Darrell. Adversarial discriminative domain adaptation. In *Computer Vision and Pattern Recognition (CVPR)*, volume 1, page 4, 2017. [7](#)
- [44] J. Ulen, P. Strandmark, and F. Kahl. Shortest paths with higher-order regularization. *IEEE transactions on pattern analysis and machine intelligence*, 37(12):2588–2600, 2015. [6](#)
- [45] C. Villani. *Topics in optimal transportation*. Number 58. American Mathematical Soc., 2003. [2](#)
- [46] C. Villani. *Optimal transport: old and new*, volume 338. Springer Science & Business Media, 2008. [2](#)
- [47] J. Ye, P. Wu, J. Z. Wang, and J. Li. Fast discrete distribution clustering using Wasserstein barycenter with sparse support. *IEEE Transactions on Signal Processing*, 65(9):2317–2332, 2017. [1](#), [3](#)